Measurements of the Rotational Spectra of Phenol and 2-Pyrone and Computational Studies of the H-Bonded Phenol−Pyrone Dimer

Chakree Tanjaroon and Stephen G. Kukolich*

Department of Chemistry, University of Arizona, Tucson 85721-0041

Received: March 20, 2009; Revised Manuscript Received: May 28, 2009

Rotational spectra for the *a*-type transitions of phenol and *a*-type and *b*-type transitions of 2-pyrone in the ground vibrational states were measured using pulsed beam Fourier transform (PBFT) microwave spectroscopy. From the observed *a*-type spectrum of phenol, which exhibited no complicated tunneling doublet splittings, we obtained the following rotational constants: $A_0 = 5650.494(26)$, $B_0 = 2619.2323(7)$, $C_0 = 1789.8520(7)$ MHz. For 2-pyrone, the following rotational constants were obtained: $A_0 = 5677.6356(10)$, $B_0 = 2882.2458(11)$, $C_0 = 1912.13275(94)$ MHz. The centrifugal distortion constant, Δ_J, for these molecules is less than 0.2 kHz, in good agreement with our predicted, theoretical Δ_J values. Combined spectral fits using data from this work and previous data provided accurate information on the rotational and centrifugal distortion constants of these molecules. From the measured rotational constants we obtained the following inertial defects (Δ): Δ(2-pyrone) = −0.053 and Δ(phenol) = −0.031 amu Å^2. The observed negative inertial defect for these planar molecules (normally a small positive value for planar molecules) suggests that the out-of-plane vibrational potential due to the attached OH and O is highly anharmonic. From the measured inertial defect, we calculated the low frequency out-of-plane vibration to be approximately 110 cm^{-1}. Quantum chemical calculations were performed in combination with the experiments to determine the molecular and spectroscopic properties of phenol, 2-pyrone and the H-bonded, phenol−pyrone dimer. A well-defined theoretical structure was obtained for the phenol−pyrone dimer from the calculations with electron correlation. Structure optimization calculations using Møller−Plesset perturbation theory predicted a stable bent dimer structure with relatively strong interaction energy in the 28−32 kJ mol^{-1} range. This novel, phenol−pyrone dimer forms a single O···HO hydrogen bond with length about 1.87−1.93 Å, and is further stabilized by $\pi-\pi$ and CH−π interactions. Density functional theory (DFT) calculations predicted that a planar nontransition state structure would be stable, but failed to predict a stable bent structure. Experimental searches for the rotational spectrum of phenol−pyrone stable were conducted in the 4−8 GHz range, but no transitions were detected in this study. A number of microwave transitions for the phenol−phenol dimer were detected in this study and used to estimate rotational constants.

I. Introduction

Phenol and 2-pyrone are important heterocyclic ring molecules which are involved in many fundamental biochemical interactions, such as hydrogen bonding and electron or proton transfer. The π-electrons in these ring molecules are a key feature in explaining chemical reactions involving these molecular systems. These molecules and many of their derivatives are known to possess broad and potent biological activity. Studies have shown that when the π-electron charge distributions of these molecules are altered, for example, by substituting functional groups, the biochemical reactivity can change.[1,2] Because of their occurrence in biologically important molecules, these heterocycles continue to attract broad experimental and theoretical interest. Moreover, phenol and pyrone are prototype molecules for understanding complex biochemical reactions, and studying their molecular and electronic properties has provided a basis to help understand their biological reactivity. In particular, understanding the vibrational dynamics, electron or proton transfer and hydrogen bonding interactions in these molecular systems can provide fundamental knowledge about the complex mechanisms of protein folding and molecular assembly.[3−8]

Infrared and UV spectra of 2-pyrone[9,10] and phenol[11,12] have been reported previously, providing some insight into their structures and dynamics. However, high resolution spectroscopic studies on 2-pyrone are limited. Norris et. al reported the first microwave spectrum of 2-pyrone[13] about thirty years ago. Microwave spectra of phenol[14−18] had been studied from 1960 to 1975. The microwave spectrum of phenol was first observed by Kojima (ref 14), and a full isotopic substitution structure of phenol was later obtained by Larsen (ref 18). The early microwave experiments were done primarily with waveguide microwave spectroscopy, with very limited spectral resolution. In addition, because of the low sensitivity of waveguide spectrometers, weak transitions (*a*-type in phenol and *b*-type in 2-pyrone) were not observed in most cases. Most of the previously measured, ground state rotational spectra of 2-pyrone and phenol were for high *J* transitions in a high microwave frequency range. To date, significant experimental information about low *J* rotational transitions in the 4−8 GHz range of phenol and 2-pyrone were not available. For small ring molecules in general, the low *J* transitions in the ground vibrational state are less perturbed by centrifugal distortion effects. Direct microwave measurements of the low *J* transitions can help to accurately characterize the molecular geometry of these molecules. In the 2-pyrone case, where chemical synthesis

* Corresponding author, E-mail: kukolich@u.arizona.edu.

10.1021/jp902555q CCC: $40.75
Published on Web 07/17/2009

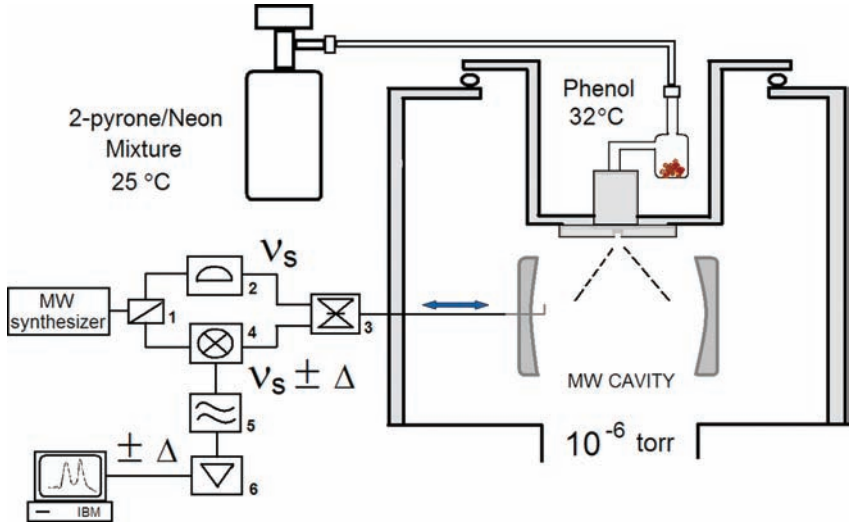

Figure 1. Diagram of the gas delivery and homodyne microwave detection system. The basic microwave electronic components are (1) Directional coupler, (2) Variable attenuator, (3) Microwave SPDT switch, (4) Double balance mixer for down conversion, (5) RF filter, (6) RF low noise amplifier. ν_s denotes microwave stimulating frequency and the Δ symbol denotes the molecular response signals.

of isotopologues is difficult, accurate measurement of the rotational constants can be used to estimate the H atom position, which could not be obtained from the crystal structure.[19]

In this work, the *a*-type microwave spectrum of the phenol molecule and the *a*-type and *b*-type microwave spectrum of 2-pyrone were studied in the 4−12 GHz microwave frequency range using a pulsed beam Fourier transform (PBFT) microwave spectrometer. Although the *b*-type spectrum of the phenol monomer was previously studied extensively, the *a*-type spectral transitions had not been observed experimentally, presumably because of the intrinsically small *a*-dipole oscillator strength (for deuterated phenol, $\mu_a = 0.13$ D[16]). Petersen et. al had attempted to measure *a*-type transitions of phenol, but no lines were detected (ref 16). The *a*-type spectrum of phenol provides precise positions of line center frequencies and is important for completely understanding the rotational energy level structure and dynamics of phenol. As with phenol, the 2-pyrone molecule has both *a*-type and *b*-type rotational spectra, but these spectra are not complicated by any proton tunneling motion. We also present here quantum chemical calculations of the molecular and spectroscopic properties of phenol and 2-pyrone for direct comparison with the new microwave experimental data. Additionally, we have used quantum chemical calculations to study the molecular properties of the hydrogen bonded phenol−pyrone dimer. Unlike Watson−Crick type base pairs,[20−23] all of which have a nearly planar structure, the predicted bent structure of phenol−pyrone is interesting because it forms a single hydrogen bond and additional stabilization energy is achieved via the $\pi-\pi$ and CH$-\pi$ interactions.

II. Experiments

Phenol (purity >99%) and 2-pyrone (2*H*-pyran-2-one: purity >90%) were purchased from Sigma-Aldrich Chemical Co. and used without further purification. About 100−200 mg of phenol (solid) and 1.0 mL of 2-pyrone (liquid) were transferred into a separate glass sample cell. For the phenol experiments, the prepared phenol cell was attached to the inlet of a pulsed nozzle which was situated inside the heating chamber. After the sample cell was securely attached, air and moisture were evacuated from the cell for a few minutes at room temperature. Following the evacuation step, neon carrier gas was let into the cell to bring the sample pressure up to about 0.8 atm. (This sample pressure was maintained throughout the experiment). The temperature inside the heated chamber was then raised to approximately 35 °C to increase the vapor pressure of the phenol sample. For the 2-pyrone experiments, sufficient pyrone was added to an evacuated, stainless steel cylinder to make a mixture of about 0.5% pyrone in 1 atm total pressure. The neon was then added to bring the total pressure up to 1 atm. This pyrone/neon gas mixture was introduced to the microwave cavity via Tygon tubing which connected the sample cylinder to the pulsed nozzle. The pyrone experiments were carried out at room temperature. To study the phenol−pyrone dimer, the prepared pyone/neon gaseous mixture was passed over the heated (25−35 °C) phenol sample.

The microwave spectra of phenol and 2-pyrone were measured using a Flygare-Balle type PBFT microwave spectrometer. Our system utilizes a homodyne (zero-IF) detection technique which heterodynes the molecular and carrier frequency signals in one mixing stage. The nozzle pulse rate was set to 1−2 Hz, and a short microwave pulse of about 1 μs was used to excite the rotational transition of the molecules. The measurements were initiated with signal optimization using the known R and Q branch transition frequencies of these molecules. Microwave pulse and trigger delays were adjusted to obtain the optimal molecular S/N ratio. Using the known *a*-type and *b*-type transitions of these molecules as a test signal, a single-shot free induction decay (FID) signal could readily be observed after optimization. We note that although the magnitude of the *a*-dipole components in phenol is only about 0.1 debye, the observed FID signal was surprisingly strong. For the phenol *a*-type $J = 1_{01} \rightarrow 0_{00}$ transition, a measurable FID signal was observed in less than ten gas pulses. The observed signal strength of the *a*-type transitions of phenol, however, was quite sensitive to the *Q* factor (Q = energy stored/energy dissipated per cycle) of the cavity resonance mode. The dipole moments of 2-pyrone were predicted to be larger than those of phenol; indeed, the signal intensity of 2-pyrone could be observed in most cases in less than 20 beam pulses. Scanning for phenol, 2-pyrone, and phenol−pyrone dimer spectra was done exclusively in the 4−12 GHz frequency range. A search for the ^{13}C spectrum of 2-pyrone in natural abundance was unsuccessful. The gas delivery and homodyne microwave detection system is shown in Figure 1.

TABLE 1: Theoretical Rotational (B_e = Equilibrium, B_0 = Vibrational Ground + Centrifugal Distortion), Asymmetrically Reduced Quartic and Sextic Centrifugal Distortion Constants and Dipole Moment for Phenol and 2-Pyrone

	phenol		2-pyrone	
molecular constant	MP2/6-311G(d)	B3LYP/6-311G(d)	MP2/6-311G(d)	B3LYP/6-311G(d)
A_e/MHz	5636.588	5671.939	5687.316	5703.680
B_e/MHz	2608.612	2618.945	2859.245	2868.327
C_e/MHz	1783.301	1791.666	1902.687	1908.540
A_0/MHz	5596.025	5629.592	5637.159	5655.361
B_0/MHz	2593.212	2602.657	2843.421	2851.646
C_0/MHz	1772.493	1779.876	1890.525	1895.928
Δ_J/kHz	0.1285	0.1287	0.1529	0.1533
Δ_{JK}/kHz	0.1809	0.1950	0.2097	0.2334
Δ_K/kHz	0.8471	0.8370	1.1627	1.1645
δ_J/kHz	0.0426	0.0425	0.0517	0.0514
δ_K/kHz	0.3438	0.3493	0.3692	0.3740
$\Phi_J/10^{-10}$MHz	0.0774	−0.0208	0.0399	0.0348
$\Phi_{JK}/10^{-10}$MHz	0.9896	2.497	0.9293	0.6518
$\Phi_K/10^{-10}$MHz	10.09	14.21	7.386	7.568
$\Phi_{KJ}/10^{-10}$MHz	−6.301	−12.14	−6.327	−5.911
$\phi_J/10^{-10}$MHz	0.0635	0.0140	0.0508	0.0539
$\phi_{JK}/10^{-10}$MHz	0.7704	1.074	0.5853	0.5352
$\phi_K/10^{-10}$MHz	4.067	2.150	5.418	5.504
Dipole moment				
a/debye	0.006	0.05	4.30	4.50
b/debye	1.46	1.42	0.86	0.81

III. Computational Studies

A. Monomers. Calculations of the molecular and spectroscopic (vibration, rotational and distortion constants) properties of phenol and pyrone were done using the Gaussian 03 electronic structure calculation program.[24] Full geometry optimizations on the structure of phenol and 2-pyrone were performed using second-order Møller−Plesset perturbation theory[25] (MP2) and density functional theory (DFT) B3LYP methods.[26] We selected relatively large triple-ζ basis sets, the Pople[27] 6-311G(d), for these geometry optimization procedures. Optional keywords, *nosymm*, *output* = *pickett*, *freq* = *anharmonic*, were selected to calculate the anharmonic frequencies and centrifugal distortion constants of these molecules. All geometry optimizations were performed in redundant internal coordinates using the default convergence and SCF criteria. The redundant internal coordinates (*xyz* coordinates) used in the geometry optimization were those for the principal axis system of the monomers. Frequency calculations were also used to check for real frequencies, to ascertain that the optimized structure is not a transition state. For the MP2 calculations, we used the same starting geometry as in the DFT calculations and the default optimization settings were used. Basis set evaluations for the best geometry were not performed for these monomers in the present work since there were excellent computational papers available on this topic.[28] We had tested one large basis set with diffuse and polarization functions (6-311++G(d,p)), to optimize the phenol structure, and it produced only a small change in rotational constants. The rotational and centrifugal distortion constants obtained from these calculations are given in Table 1. Figure 2 shows the basic molecular structures of phenol and 2-pyrone in their principal inertial axis systems.

B. Phenol−Pyrone Dimer. The molecular structure of H-bonded phenol−pyrone dimer was studied using MP2 methods. Kolář and Hobza have shown that the MP2 method with medium atomic orbital basis sets is required to obtain a reliable geometry for this type of weakly H-bonded complex.[29] We chose double-ζ 6-31+G(d,p) and cc-pVDZ basis sets to describe the atomic orbitals. This 6-31G[30] medium basis set has been shown to give similar performance in geometry optimization as the pVDZ[31] and correlation consistence cc-pVDZ[32] basis sets, even for systems with a large number of electrons. The starting geometry used in this MP2 optimization calculation was a planar configuration. Harmonic frequency calculations were performed following optimization to check that the optimized structure of dimer lies at a potential minimum and to estimate the harmonic zero point energy (ZPE). Anharmonic frequency analyses were not carried out due to the increased complexity

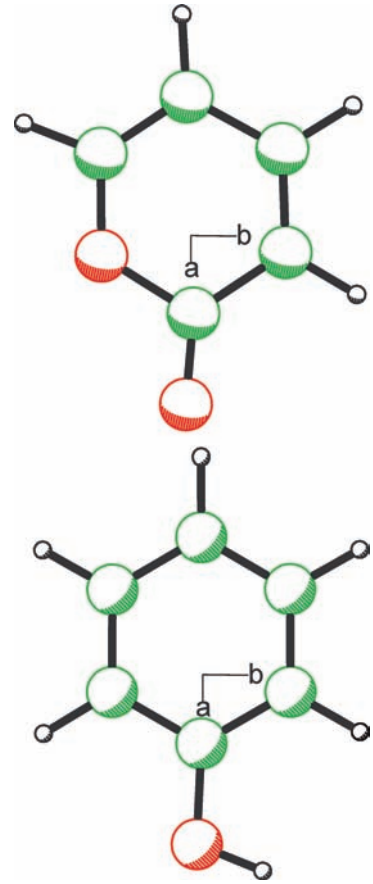

Figure 2. Calculated molecular structures for the ground-state phenol and 2-pyrone, indicating the principal inertial axis system.

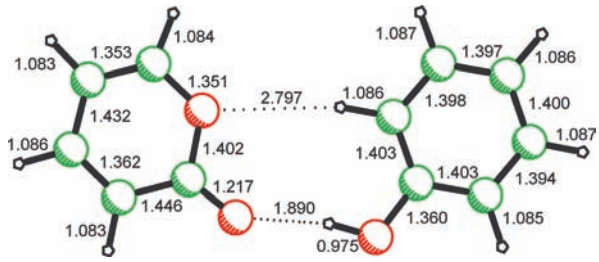

Figure 3. The planar structure of the phenol−pyrone dimer obtained from B3LYP/6-31+G(d,p) calculations. The bond distances are in angstroms.

in molecular structure and large number of degrees of freedom. All optimization procedures were done at default SCF settings. The converged bent geometry had two very low imaginary frequencies (ring flapping = 6i cm^{-1} and ring twisting = 23i cm^{-1}). These low frequency intermolecular vibrations closely resemble restricted translations and internal rotations. This structure is not a true transition state and energetically, this bent geometry lies slightly above the true minimum. By using the *counterpoise* keyword option in Gaussian 03, the counterpoise corrected interaction energy for the dimer was evaluated as $\Delta E_{CP} = E_{Cp\text{-}corrected}(dimer) - [E_{MCB}(phenol) + E_{MCB}(pyrone)]$, an equation based on the supermolecule method.[33] The dissociation energy of the dimer was calculated using the following equation: $D_0 = -\Delta E_{CP} - (ZPE_{dimer} - ZPE_{phenol} - ZPE_{pyrone})$. To study the effect and illustrate the importance of electron correlation, we optimized the structure of the dimer using density function theory, a method without electron correlation, with the B3LYP/6-31+G(d,p) level of calculation. Figures 3 and 4 show the optimized structure of the dimer with the corresponding bond distance obtained from B3LYP and MP2. Table 2 lists the calculated molecular constants, inertial defect and binding energy for the dimer.

IV. Spectral Analysis and Results

A. Phenol and 2-Pyrone. We have measured and analyzed the weak *a*-type microwave spectrum of phenol to obtain the rotational and centrifugal distortion constants. Unlike the *b*-type transitions, the observed *a*-type transitions yield single peaks; thus, more precise frequencies can be determined for these lines. These *a*-type transitions are not expected to show OH-torsional splitting because the internal rotation of the OH group has no effect on the *a*-dipole moment. The *a*-dipole moment lies approximately along the C−O bond of the monomer. For the *b*-type spectrum, the OH-torsional motion splits the observed lines of phenol into doublets. Previous microwave experiments and theoretical studies of OH torsional barriers (refs 14−18) showed that, for *b*-type transitions, the *A* and *B* torsional transitions were split by about 112 MHz. Some of the *b*-type lines were observed in our experiments and they were split by about 112 MHz. The observed *a*-type transitions were fit using SPFIT and SPCAT[34] spectral fitting programs. Rotational energy diagonalization was done using Watson's *a*-reduced Hamiltonian with the Δ_J quartic centrifugal distortion term.[35] In the current fit, because of limited numbers of observed transitions, the other quartic distortion constant terms could not be determined and were fixed to zero. The measured *a*-type transitions for phenol and the fit residuals (measured frequency − calculated frequency) are given in Table 3. Table 4 lists the spectroscopic constants of phenol obtained from this least-squares fit analysis.

Analysis of the spectrum of 2-pyrone was straightforward. The assignment of transitions was done using the same distortable Hamiltonian as used for the analysis of the phenol spectrum. Because more lines were observed for 2-pyrone, it was possible to determine the quartic distortion constants Δ_J and δ_J. Other quartic centrifugal distortion terms however could not be fit and were fixed to zero. The measured *a*-type and *b*-type transitions for 2-pyrone and the fit residuals are given in Table 5. Table 6 lists the spectroscopic constants of 2-pyrone from the fit.

Combined fits using data from this work and previous microwave work were carried out for the monomers. For phenol, a total of 46 distinct transitions were fit, including 8 *a*-type (this work) and 38 *b*-type center lines (ref 17). For 2-pyrone, 30 distinct transitions were fit by combining data from this work with those of ref 13. The combined fit, which required some sextic distortion constants, yielded standard deviations on the order of 10−20 kHz. The larger fit deviation may be attributed to limited spectral line resolution (0.1 MHz) for the previous measurements, which limited the measurement precision to about 0.01 MHz. These fit results are given in Tables 4 and 6.

B. Search for a Phenol−Pyrone Dimer and Detection of a Phenol−Phenol Dimer. Using our predicted rotational constants for the phenol−pyrone dimer, we initiated an extensive search for phenol−pyrone dimer transitions in the 4−8 GHz frequency range. Our calculations predicted a set of $J = 3-4$ and $J = 2-3$ strong *b*-type transitions (about 3.8 debye) in the 7 GHz region, where we initially focused our search. Extra lines (about 30 lines) which were not due to monomers were observed during the experimental scans. From our control studies, in which we omitted either phenol or 2-pyrone from the sample mixtures, it was subsequently verified that these lines were not the right spectral carrier of the H-bonded phenol−pyrone dimer. Further analysis indicated that some of these new lines could be the phenol−phenol dimer lines. From the observed asymmetry splitting pattern of these phenol−phenol lines, we estimated the rotational constants to be $A = 1413.15$, $B = 314.09$, and $C = 290.04$ MHz, which agreed well with the values obtained from high resolution electronic spectroscopy.[36−39] Attempts to fit these phenol−phenol lines however were not entirely successful. Although a reasonable fit (using 15−20 lines) could be obtained using a large number of distortion parameters, we believe that these fits did not provide a definitive assignment.

V. Discussion

Using the pulsed beam Fourier transform microwave spectrometer with a homodyne direct detection technique, we have measured the *a*-type microwave spectrum of phenol and *a*-type and *b*-type microwave spectrum of the 2-pyrone in the 4−12 GHz frequency range. The results of our experimental studies of phenol and 2-pyrone are in good agreement with the data reported from previous experimental studies. The experimental rotational constants obtained for 2-pyrone are about 1.0% smaller than those calculated from the crystal structure (the C−H bond is fixed to a theoretical value of 1.08 Å). We attributed these differences in the values of rotational constants primarily to crystal packing effects in the crystal structure. There is a small uncertainty due to the assumed (theoretical values) C−H bond distance and angles. Varying the C−H bond distance in the X-ray structure from 1.08 to 1.85 Å has negligible effect on the rotational constants. The measured rotational constants of the monomers also agreed well with the computed rotational constants obtained from MP2 and B3LYP calculations. The theoretical calculations provided B_0 (rotational constants in the ground vibration + centrifugal distortion) values that agreed

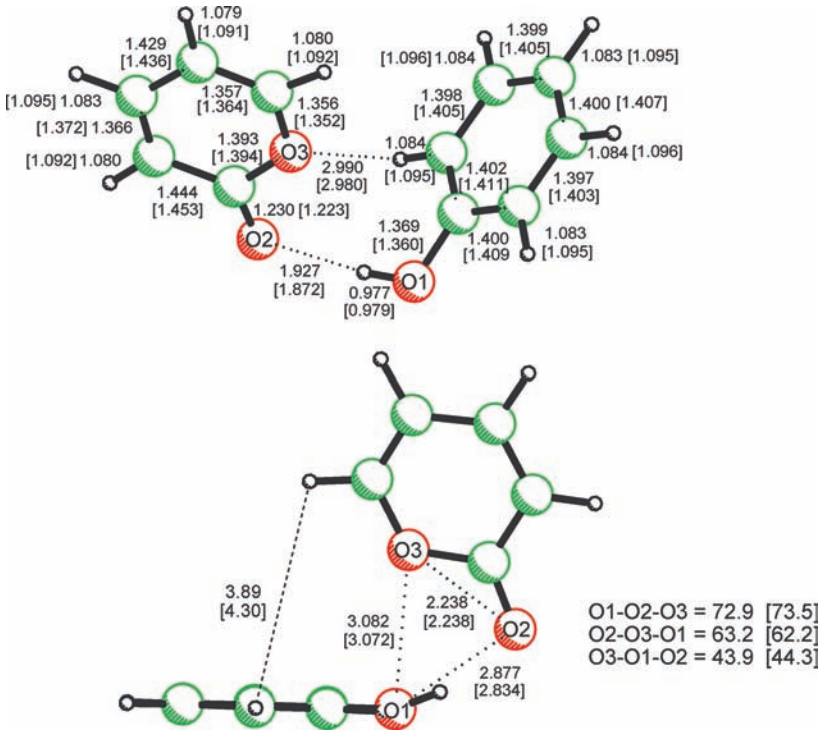

Figure 4. The bent structure of the phenol−pyrone dimer obtained from MP2 calculations. The denoted bond distance and angle with/without bracket correspond to the atomic basis functions 6-31+G(d,p)/[cc-pVDZ] used in the calculations. Also shown is the distance $R_{CH-\pi} = 3.89$ [4.03] Å, measuring from the centroid of phenol ring to the nearest interacting H atom of 2-pyrone. The bond distances are in angstroms and the ∠O-O-O angles are in degrees.

TABLE 2: Theoretical Rotational Constants and Inertial Defect (Δ) = ($I_C - I_A - I_B$) amu Å^2 for the Phenol−Pyrone Dimer[a]

	phenol−pyrone		
molecular constant	B3LYP/6-31+G(d,p)	MP2/6-31+G(d,p)	MP2/cc-pVDZ
A_e/MHz	1817.9455	1320.8495	1356.1787
B_e/MHz	262.5375	404.1153	381.6672
C_e/MHz	229.4077	356.2669	345.4322
Δ	0.0002		
ΔE_{CP}/cm^{-1}	2330	2708	2322
ΔE_{CP}/kJ mol^{-1}	27.9	32.4	27.8
D_0/cm^{-1}	1910	2177	
D_0/kJ mol^{-1}	22.9	26.2	
structure	planar	bent	bent

[a] The calculated counterpoised corrected interaction energy (ΔE_{CP}) is reported as a positive value, and the dissociation energy (D_0) is calculated using equations given in section III.

TABLE 3: Measured *a*-Type Transition Frequencies and Measurement Errors (Numbers in Parentheses Are in Units of the Last Significant Figure) for Phenol (C_6H_5OH)[a]

$J'_{Ka'Kc'}$	$J''_{Ka''Kc''}$	measd(error)	measd − calcd
1_{01}	0_{00}	4409.0825(45)	−0.0013
3_{12}	3_{13}	4959.4302(71)	0.0028
2_{12}	1_{11}	7988.7827(43)	−0.0022
4_{13}	4_{14}	8178.0195(76)	−0.0022
2_{02}	1_{01}	8670.0453(35)	0.0012
2_{11}	1_{10}	9647.5477(43)	0.0020
3_{13}	2_{12}	11897.5898(66)	−0.0008
3_{03}	2_{02}	12663.5570(73)	0.0005

[a] Values are given in MHz.

with the experimental values to better than 1%. The observed small centrifugal distortion constants show that the structures of phenol and 2-pyrone are reasonably rigid in the ground vibrational state. As seen in Table 5, the measured centrifugal distortion constant Δ_J for phenol and 2-pyrone is much less than 1 kHz. For both molecules the value of the fit quartic distortion constants agreed well with our calculated theoretical values. The similar values of rotational and centrifugal distortion constants observed for phenol and 2-pyrone indicate that the distribution of rotational energies is nearly identical for both molecules, as seen in Figure 5. At higher *J*-values, however, the asymmetry splittings are expected to spread out more for 2-pyrone due to its heavier total mass.

From the observed inertial defect (Δ), it is interesting to note that 2-pyrone is indicated to be slightly less planar than phenol. The observed negative inertial defect for these planar molecules indicates the existence of low frequency, large amplitude, anharmonic out-of-plane bending vibrations. T. Oka[40] has studied the cause of negative inertial defects and shown that for aromatic molecules the following empirical relation applies: $\Delta = -33.715/\nu_1 + 0.0186(I_{CC})^{1/2}$. The expression relates the negative inertial defect to a low frequency out-of-plane vibrational motion. In planar molecules like phenol and 2-pyrone, the frequency of these out-of-plane vibrations is much less than the frequency of in-plane vibrations. For phenol, it is believed that the low frequency torsional out-of-plane vibration of OH causes the negative inertial defect. The large ($\Delta > 0.05$ amu Å^2) negative inertial defect observed for 2-pyrone is unusual, and we suspect a large amplitude out-of-plane vibration of the heavy, oxygen atoms. Figure 6 shows the lowest out-of-plane frequency bending modes for phenol and 2-pyrone as computed from anharmonic frequency calculations. From the observed inertial defect, we calculated the low frequency out-of-plane vibrations for phenol = 108 cm^{-1} and 2-pyrone = 111 cm^{-1}. The average value of these two frequencies is about 110 cm^{-1}. For 2-pyrone, relatively good agreement between the experimental and theoretical frequencies for the low frequency

TABLE 4: Spectroscopic Constants for Phenol (This Work) Obtained from Fitting the Data in Table 3[a]

constant	this work	combined fit[b]	ref 17	ref 18	ref 14
A_0/MHz	5650.494(26)	5650.5226(49)	5650.521(5)	5650.5154(11)	5650.46(20)
B_0/MHz	2619.2323(7)	2619.2381(18)	2619.239(2)	2619.2360(5)	2619.20(20)
C_0/MHz	1789.8520(7)	1789.8540(18)	1789.855(2)	1789.8520(3)	1789.84(20)
Δ_J/kHz	0.100(53)	0.165(29)	0.160	0.1340	
Δ_{JK}/kHz		0.70(42)	0.268	−0.4291	
Δ_K/kHz		0.74(19)	0.887	1.487	
δ_J/kHz		0.044(11)	0.046	0.0442	
δ_K/kHz		0.29(25)	0.305	0.0147	
Φ_{JK}/MHz		0.0000071(53)			
Φ_{KJ}/MHz		−0.0000041(38)			
Φ_K/MHz		0.0000083(70)			
Δ	−0.031	−0.031	−0.030	−0.030	−0.032
ν_1/cm^{-1}	108	108	108	108	108
σ(fit)/kHz	2	23			

[a] The standard fit errors in the parentheses are at 1σ (67% confidence level), in units of the last significant figure. σ (fit) denotes the standard deviation of the fit. Inertial defect (Δ) = ($I_C - I_A - I_B$) amu Å^2. The calculated empirical large amplitude, low frequency out-of-plane vibration ν_1 is calculated using $\Delta = -33.715/\nu_1 + 0.0186(I_{CC})^{1/2}$. [b] Combined fit combined *a*-type lines in Table 3 with the *b*-type center lines of ref 17 (46 distinct lines in total). The quartic distortion constants from ref 18 were calculated from the τ's distortion constants. (Conversion formulas can be found in the following papers: Watson, J. K. G. In *Vibrational Spectra and Structure*; During, J. R., Ed.; Elsevier: Amsterdam, 1977; Vol. 6. Oka, T.; Morino, Y. *J. Phys. Soc. Jpn.* **1961**, *16*, 1235.)

TABLE 5: Measured Rotational Frequencies and Measurement Errors (Numbers in Parentheses Are in Units of the Last Significant Figure) for 2-Pyrone ($C_4H_4O_2$) in the Ground Vibrational State[a]

$J'_{Ka'Kc'}$	$J''_{Ka''Kc''}$	measd(error)	measd − calcd
1_{01}	0_{00}	4794.3758(36)	−0.0021
2_{11}	2_{02}	4947.3662(43)	0.0039
3_{12}	3_{13}	5790.9326(34)	−0.0029
2_{02}	1_{11}	6581.6089(40)	−0.0048
3_{12}	3_{03}	7040.1636(22)	0.0035
1_{11}	0_{00}	7589.7727(30)	0.0047
3_{21}	3_{12}	8080.9473(43)	−0.0080
2_{20}	2_{11}	8597.9191(31)	−0.0003
2_{12}	1_{11}	8618.6398(26)	−0.0007
2_{02}	1_{01}	9377.0043(35)	0.0004
4_{13}	4_{14}	9498.9252(19)	0.0005
4_{13}	4_{04}	10156.6927(35)	−0.0010
2_{11}	1_{10}	10558.8617(40)	−0.0017
2_{21}	2_{12}	11296.5078(46)	0.0010
2_{12}	1_{01}	11414.0352(34)	0.0046
3_{03}	2_{12}	11558.1752(30)	0.0005

[a] Values are given in MHz.

TABLE 6: Spectroscopic Constants for the Ground State Structure of 2-Pyrone (This Work) Obtained from Fitting the Data Given in Table 5[a]

constant	this work	combined fit[b]	ref 13	ref 19[c]
A_0/MHz	5677.6356(10)	5677.6378(30)	5677.643(20)	5780.1513
B_0/MHz	2882.2458(11)	2882.2451(12)	2882.240(5)	2915.6317
C_0/MHz	1912.13275(94)	1912.1316(12)	1912.133(3)	1938.6423
Δ_J/kHz	0.161(75)	[0.161]		
Δ_{JK}/kHz		0.322(86)		
δ_J/kHz	0.050(15)	0.0672(46)		
Φ_J/MHz		0.0000108(24)		
Δ	−0.053	−0.053	−0.053	−0.081
ν_1/cm^{-1}	111	111	111	88
σ(fit)/kHz	3	13		

[a] The standard fit errors in the parentheses are at 1σ (67% confidence level), in units of the last significant figure. The σ(fit) denotes the standard deviation of the fit. Inertial defect (Δ) = ($I_C - I_A - I_B$) amu Å^2. The calculated empirical large amplitude, low frequency out-of-plane vibration ν_1 is calculated using $\Delta = -33.715/\nu_1 + 0.0186(I_{CC})^{1/2}$. [b] Combined fit combined lines in Table 5 with the *a*-type and *b*-type lines of ref 13 (30 distinct lines in total). [c] Calculated from the X-ray diffraction geometry with R_{C-H} fixed at 1.08 Å with the H atoms constrained in the *ab*-plane of the carbon atoms.

out-of-plane bending modes was found. A large discrepancy for the vibrational modes, however, was observed for phenol. Calculated frequencies were about twice the experimental values.

$\pi-\pi$ type interactions between two aromatic rings are known to provide a driving force for the DNA base stacking interactions.[41−43] It is also known that interactions between aromatic rings with hydrogen bonding capability can produce either base stacking or planar complexes.[44] Our electron correlation calculations have predicted that the H-bonded phenol−pyrone species is a bent complex with reasonably strong interaction energy. The bent dimer forms a single O···HO hydrogen bond with bond lengths of about 1.93 Å (MP2/6-31+G(d,p)) or 1.87 Å (MP2/cc-pVDZ). The correlation consistent cc-pVDZ basis set predicts an O···HO hydrogen bond distance that is 0.06 Å shorter than that of the 6-31+G(d,p) basis set. Overall, these MP2 calculations using medium atomic basis orbitals have yielded a nearly identical phenol−pyrone structure. This bent structure motif is an example of a sterically favorable complex. From our calculations, it is clear that the dispersion interactions involving $\pi-\pi$ and CH$-\pi$ interactions (as evidence from twisting and bending of the ring) played a significant role in stabilizing the overall interaction energy of the complex. The planar structure predicted using DFT (B3LYP/6-31+G(d,p)) may not be reliable because DFT calculations do not accurately describe the weak electrostatic and dispersion interactions, such as $\pi-\pi$ and CH$-\pi$ interactions.

Our MP2 calculation predicted the interaction energy (not including ZPE correction) in the range of about $\Delta E_{CP} = 28-32$ kJ mol^{-1} for the bent phenol−pyrone dimer. This value is the same order of magnitude as was calculated for the aromatic phenol−phenol dimer. The calculated interaction energy (including the ZPE correction) for phenol−phenol is about 32.3 kJ mol^{-1} (ref 34). Because phenol−phenol and phenol−pyrone dimers have nearly identical interaction energies, these H-bonded species could both be present as two separate molecular complexes in molecular beams. Although, these dimers have similar rotational constants, the predicted spectra of these dimers are clearly distinct. Even if there were some partial and accidental overlapping of lines, many of the transitions appear

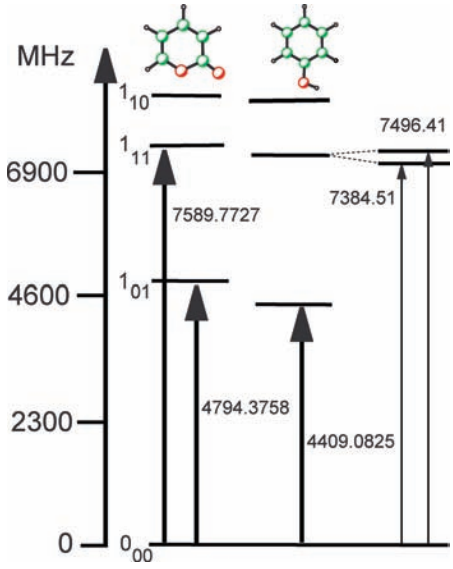

Figure 5. A schematic representation of the lowest rotational energy levels and observed rotational transitions for phenol and 2-pyrone. From the ground rotational state, the first rotational energy level (J_{KaKc}) is $1_{01} = B + C$ MHz, the second level is $1_{11} = A + C$ MHz, and the third level is $1_{10} = A + B$ MHz. The transition from the ground rotational level to $1_{10} = A + B$ MHz is forbidden by the dipole selection rule. The thinner arrows illustrate the phenol *b*-type doublet transitions as reported in ref 17.

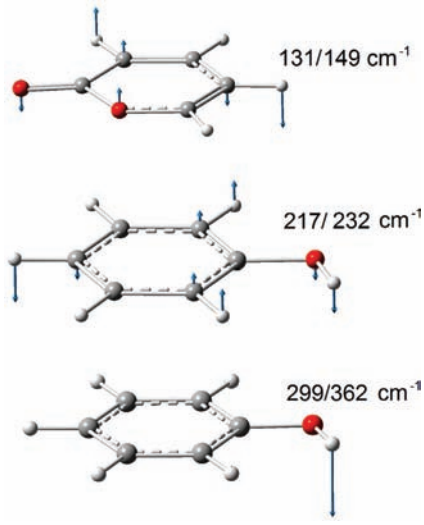

Figure 6. Low frequency out-of-plane bending vibration of the ring for the equilibrium structures of phenol and 2-pyrone obtained from anharmonic frequency calculations. Also shown is the low frequency OH out-of-plane torsional mode of phenol. The denoted values (value1/value2) correspond to MP2/B3LYP. From the measured inertial defect, the experimental low frequency out-of-plane vibration values are approximately phenol = 108 cm^{-1} and 2-pyrone 111 cm^{-1}.

well separated. The fact that we did not observe any phenol−pyrone dimer lines suggests perhaps there is a problem with our experimental conditions. The calculated interaction energy for phenol−phenol should be stronger than that of the phenol−pyrone dimer. This suggests the presence of phenol−phenol dimer could quench the production of phenol−pyrone dimer in molecular beams. One solution to this problem is to limit the phenol concentration in the molecular beam to low values (preferably <0.25%), which we have tried with limited success. In our experiments we control the concentration of phenol by varying the temperature in the thermal chamber, but it is difficult to maintain the precise and constant concentrations this way. Thus far, we have been unable to observe the phenol−pyrone transitions to confirm our theoretical results.

VI. Conclusions

The weak *a*-type rotational transitions of phenol and the *a*-type and *b*-type rotational transitions of 2-pyrone were measured in the 4−12 GHz range using PBFT microwave spectroscopy with a homodyne direct detection technique.[45] Analysis of this new, high resolution microwave data, in combination with the previous microwave data, has yielded accurate values of the ground state rotational and centrifugal distortion constants for phenol and 2-pyrone. Evaluation of the inertial defect yielded new information about a low frequency out-of-plane bending vibration, which we calculated to be on the order of 100 cm^{-1} for both molecules in the ground state. An experimental effort was made to measure the rotational spectrum of the H-bonded phenol−pyrone dimer, but no phenol−pyrone lines were observed in this experiment. A number of rotational transitions of phenol−phenol dimer were observed in this experiment, allowing us to estimate its rotational constants. However, a definite assignment of the observed phenol−phenol lines has not yet been achieved due to the spectral complexity. Computational studies of the structure and spectroscopic properties of phenol, 2-pyrone, and the hydrogen bonded phenol−pyrone dimer were carried out to help guide and interpret the new experimental data. In the case of phenol−pyrone dimer, the results of these calculations suggest the structure of phenol−pyrone is bent. Calculations using MP2 with medium atomic basis sets further shows that the bent species has fairly high interaction energy, and the stability is achieved not only through the hydrogen bonding but via the $\pi-\pi$ and CH$-\pi$ dispersion interactions. Higher level electronic structure calculations may provide accurate details about the molecular and spectroscopic properties of this interesting, yet elusive H-bonded complex.

Acknowledgment. This material is based upon work supported by the National Science Foundation under Grant No. CHE-0721505 and Grant No. CHE-0809053. We are very grateful to the NSF for providing funding for this research. We thank the referees for their constructive comments and suggestions.

References and Notes

(1) Fairlamb, I. J. S.; Marrison, L. R.; Dickinson, J. M.; Lu, F.-J.; Schmidt, J. P. *Bioorg. Med. Chem.* **2004**, *12*, 4285.
(2) Suarez, D.; Menendez, J. A.; Fuente, E.; Montes-Moran, M. A. *Langmuir* **1999**, *15*, 3897.
(3) Kayano, M.; Ebata, T.; Yamada, Y.; Mikami, N. *J. Chem. Phys.* **2004**, *120*, 7410.
(4) Benoit, D. M.; Clary, D. C. *J. Phys. Chem. A* **2000**, *104*, 5590.
(5) Watanabe, H.; Iwata, S. *J. Chem. Phys.* **1996**, *105*, 420.
(6) Kwac, K.; Lee, C.; Jung, Y.; Han, J.; Kwak, K.; Zheng, J.; Fayer, M. D.; Cho, M. *J. Chem. Phys.* **2006**, *125*, 244508.
(7) Sobolewski, A. L.; Domcke, W. *J. Phys. Chem. A* **2001**, *105*, 9275.
(8) Ebata, T.; Fujii, A.; Mikami, N. *Int. Rev. Phys. Chem.* **1998**, *17*, 331.
(9) Fausto, R.; Quinteiro, G.; Breda, S. *J. Mol. Struct.* **2001**, *598* (2−3), 287.
(10) de Melo, J. S.; Quinteiro, G.; Pina, J.; Breda, S.; Fausto, R. *J. Mol. Spectrosc.* **2001**, *565*−*566*, 59.
(11) Michalska, D.; Zierkiewicz, W.; Bienko, D. C.; Wojciechowski, W.; Zeegers-Huyskens, T. *J. Phys. Chem. A* **2001**, *105*, 8734.
(12) Rospenk, M.; Leroux, N.; Zeegers-Huyskens, T. *J. Mol. Spectrosc.* **1997**, *183*, 245.
(13) Norris, C. L.; Benson, R. C.; Beak, P.; Flygare, W. H. *J. Am. Chem. Soc.* **1973**, *95*, 2766.
(14) Kojima, T. *J. Phys. Soc. Jpn.* **1960**, *15*, 284.
(15) Forest, H.; Dailey, B. P. *J. Chem. Phys.* **1966**, *45*, 1736.

(16) Pedersen, T.; Larsen, N. W.; Nygaard, L. *J. Mol. Struct.* **1969**, *4*, 59.

(17) Mathier, E.; Welti, D.; Bauder, A.; Günthard, Hs. H. *J. Mol. Spectrosc.* **1971**, *37*, 63.

(18) Larsen, N. W. *J. Mol. Struct.* **1975**, *51*, 175.

(19) Blake, A. J.; Gould, R. O.; Harris, S. G.; McNab, H.; Parsons, S. *Acta Crystallogr.* **1994**, *C50*, 1938.

(20) Roscioli, J. R.; Pratt, D. W. *Proc. Natl. Acad. Sci. U.S.A.* **2003**, *100*, 13752.

(21) Borsta, D. R.; Roscioli, J. R.; Pratt, D. W.; Floriob, G. M.; Zwier, T. S.; Müllerc, A.; Leutwyler, S. *Chem. Phys.* **2002**, *283*, 341.

(22) Müller, A.; Talbot, F.; Leutwyler, S. *J. Chem. Phys.* **2001**, *115*, 5192.

(23) Matsuda, Y.; Ebata, T.; Mikami, N. *J. Chem. Phys.* **2000**, *113*, 573.

(24) Frisch, M. J.; Trucks, G. W.; Schlegel, H. B.; Scuseria, G. E.; Robb, M. A.; Cheeseman, J. R.; Montgomery, J. A.; Jr., Vreven, T.; Kudin, K. N.; Burant, J. C.; Millam, J. M.; Iyengar, S. S.; Tomasi, J.; Barone, V.; Mennucci, B.; Cossi, M.; Scalmani, G.; Rega, N.; Petersson, G. A.; Nakatsuji, H.; Hada, M.; Ehara, M.; Toyota, K.; Fukuda, R.; Hasegawa, J.; Ishida, M.; Nakajima, T.; Honda, Y.; Kitao, O.; Nakai, H.; Klene, M.; Li, X.; Knox, J. E.; Hratchian, H. P.; Cross, J. B.; Bakken, V.; Adamo, C.; Jaramillo, J.; Gomperts, R.; Stratmann, R. E.; Yazyev, O.; Austin, A. J.; Cammi, R.; Pomelli, C.; Ochterski, J. W.; Ayala, P. Y.; Morokuma, K.; Voth, G. A.; Salvador, P.; Dannenberg, J. J.; Zakrzewski, V. G.; Dapprich, S.; Daniels, A. D.; Strain, M. C.; Farkas, O.; Malick, D. K.; Rabuck, A. D.; Raghavachari, K.; Foresman, J. B.; Ortiz, J. V.; Cui, Q.; Baboul, A. G.; Clifford, S.; Cioslowski, J.; Stefanov, B. B.; Liu, G.; Liashenko, A.; Piskorz, P.; Komaromi, I.; Martin, R. L.; Fox, D. J.; Keith, T.; Al-Laham, M. A.; Peng, C. Y.; Nanayakkara, A.; Challacombe, M.; Gill, P. M. W.; Johnson, B.; Chen, W.; Wong, M. W.; Gonzalez, C.; and Pople, J. A. *Gaussian 03, Revision C.02*; Gaussian, Inc.: Wallingford, CT, 2004.

(25) Moller, C.; Plesset, M. S. *Phys. Rev.* **1934**, *46*, 618. Head-Gordon, M.; Pople, J. A.; Frisch, M. J. *Chem. Phys. Lett.* **1988**, *153*, 503.

(26) Becke, A. D. *J. Chem. Phys.* **1996**, *104*, 1040. Yang, L. W.; Parr, R. G. *Phys. Rev. B* **1988**, *37*, 785. Miehlich, B.; Savin, A.; Stoll, H.; Preuss, H. *Chem. Phys. Lett.* **1989**, *157*, 200.

(27) Ditchfield, R.; Hehre, W. J.; Pople, J. A. *J. Chem. Phys.* **1971**, *54*, 724. Krishnan, R.; Binkley, J. S.; Seeger, R.; Pople, J. A. *J. Chem. Phys.* **1980**, *72*, 650. McLean, A. D.; Chandler, G. S. *J. Chem. Phys.* **1980**, *72*, 5639.

(28) Kim, K.; Jordan, K. D. *Chem. Phys. Lett.* **1994**, *218*, 261.

(29) Kolář, M.; Hobza, P. *J. Phys. Chem. A* **2007**, *111*, 5851.

(30) Rassolov, V. A.; Ratner, M. A.; Pople, J. A.; Redfern, P. C.; Curtiss, L. A. *J. Comput. Chem.* **2001**, *22*, 976.

(31) Shafer, A.; Horn, H.; Ahlrichs, R. *J. Chem. Phys.* **1992**, *97*, 2571.

(32) Wilson, A. K.; Woon, D. E.; Peterson, K. A.; Dunning, T. H., Jr. *J. Chem. Phys.* **1999**, *110*, 7667.

(33) Boys, S. F.; Bernardi, F. *Mol. Phys.* **1970**, *19*, 553.

(34) Pickett, H. M. *J. Mol. Spectrosc.* **1991**, *148*, 371 (see also http://spec.jpl.nasa.gov/ftp/pub/calpgm/spinv.html).

(35) Watson, J. K. G. *J. Chem. Phys.* **1967**, *46*, 1935.

(36) Connell, L. L.; Ohline, S. M.; Joireman, P. W.; Corcoran, T. C.; Felker, P. M. *J. Chem. Phys.* **2001**, *92*, 2585.

(37) Weichert, A.; Riehn, C.; Brutschy, B. *J. Phys. Chem. A* **2001**, *105*, 5679.

(38) Schmitt, M.; Böhm, M.; Ratzer, C.; Krügler, D.; Kleinermanns, K.; Kalkman, I.; Berden, G.; Meerts, W. L. *ChemPhysChem* **2006**, *7*, 1241.

(39) Brause, R.; Santa, M.; Schmitt, M.; Kleinermanns, K. *ChemPhysChem* **2007**, *8*, 1394.

(40) Oka, T. *J. Mol. Struct.* **1995**, *352/353*, 225.

(41) Mishra, B. K.; Sathyamurthy, N. *J. Phys. Chem. A* **2005**, *109*, 6.

(42) Tsuzuki, S.; Honda, K.; Uchimaru, T.; Mikami, M.; Tanabe, K. *J. Am. Chem. Soc.* **2004**, *124*, 104.

(43) Sinnokrot, M.; Valeev, E. F.; Sherrill, C. D. *J. Am. Chem. Soc.* **2002**, *124*, 10887.

(44) Hobza, P.; Sponer, J.; Polasek, M. *J. Am. Chem. Soc.* **1995**, *117*, 792.

(45) Tackett, B. S.; Karunatilaka, C.; Daly, A.; Kukolich, S. G. *Organometallics* **2007**, *26*, 2070–2076.

JP902555Q